On the role of additive manufacturing, heat treatment and machining on the microstructural evolution and corrosion behaviour of AlSi9Cu3(Fe) alloy

Research Article Vol. 30, No. 9 / 25 Apr 2022 / Optics Express 14341
Optics EXPRESS

Study of nonlinear effects and self-heating in a silicon microring resonator including a Shockley-Read-Hall model for carrier recombination

MARCO NOVARESE,[1,*] SEBASTIAN ROMERO GARCIA,[2] STEFANIA CUCCO,[1] DON ADAMS,[3] JOCK BOVINGTON,[3] AND MARIANGELA GIOANNINI[1]

[1]Department of Electronics and Telecommunications, Politecnico di Torino, 10129 Torino, Italy
[2]Cisco Optical GmbH, Nuremberg, Germany
[3]Cisco Systems, San Jose, CA 95134, USA
[*]marco.novarese@polito.it

Abstract: A detailed description of the non-linear effects in silicon is needed when designing ring resonators in the silicon platform. The optical field propagating in the ring waveguide is strongly absorbed due to two-photon-absorption (TPA) and free-carrier-absorption (FCA), which become more prominent with increasing the input power in the ring. We present a new approach for the modelling of non-linear effects in silicon based ring resonators. We have numerically solved the non-linear problem coupling the variation of refractive index and loss due to TPA, FCA , self-heating and Shockley-Read-Hall (SRH) theory for trap-assisted recombination process. The model is validated by reproducing experimental measurements on a ring and a racetrack resonator having different Q-factors and waveguide cross-sections. As a result, we show that the SRH recombination is the origin of the dependence of free carrier lifetime on the power circulating in the ring and how this dependence is affected by the surface trap density and trap energy level. The model is then applied to the calculation of the maximum power that can incident the silicon rings designed for the Si PIC mirror of a hybrid III-V/Si widely tunable laser.

1. Introduction

Many silicon photonic integrated circuits rely on the Silicon-on-Insulator platform thanks to its compatibility with CMOS process. The use of the silicon device layer for the realization of components such as optical waveguides and ring resonators has the advantage, with respect to the silicon nitride counterpart, of assuring a stronger field confinement in the silicon core with superior miniaturization, reduced bend loss, and very small ring resonators [1]. In addition, silicon has a thermo-optic coefficient which is about seven times larger than in the silicon nitride case [2,3]; silicon micro-ring resonators are therefore preferred when a wide thermal tuning of the ring resonant wavelength is required. However silicon is affected, in both C- and O-band, by strong non-linear effects which cause a wavelength shift and distortion of the ring spectral response [4–7] when the power injected in the ring increases. Two-photon-Absorption (TPA) and Free-Carrier-Absorption (FCA) are the main mechanism responsible for such behaviour [5]. In TPA, two photons are absorbed generating an electron-hole pair; the generated free-carriers cause a change in the refractive index (blue shift) called free-carrier dispersion (FCD) and contribute to higher absorption (FCA) rising the overall optical loss and reducing the quality factor of the resonator. These carriers recombine releasing the energy in form of heat (self-heating) which leads to an important temperature increase in the ring cross section, thermal refractive index change and red shift of the ring resonance. At low input power however also linear loss can be a cause of self-heating as for example assumed in [5] and [4] because a fraction of the power lost is

#446739 https://doi.org/10.1364/OE.446739
Journal © 2022 Received 26 Oct 2021; revised 17 Mar 2022; accepted 17 Mar 2022; published 14 Apr 2022

Optics EXPRESS

absorbed by silicon (due to for example surface state absorption [8]) instead of being radiated in the cladding.

Silicon non-linearities are detrimental in applications where rings are utilized as narrow band mirrors in tunable high power hybrid lasers [9] because a significant amount of power (proportional to the finesse of the ring) is stored in the ring even when just a few milliwatts are incident from the laser gain section. For this application, the ring spectral response should remain as close as possible to the one in linear regime. The amount of spectral distortion in the ring response is determined by the density of free-carriers accumulated in the conduction and valence band, and also by the temperature increase, which is proportional to the thermal impedance of the ring for the same amount of absorbed power.

The non-radiative recombination processes in silicon determine the free carrier lifetime: a smaller lifetime implies faster recombination of free-carriers, whose reduction is then associated to lower loss; while a smaller thermal impedance is required to limit the red wavelength shift of the resonance when self-heating becomes dominant.

A careful estimation of the carrier lifetime is therefore required to predict the amount of non-linear loss, free-carrier dispersion, and power absorbed. The correct modelling of the carrier lifetime is a key requirement when we need to quantify the maximum power (incident in the ring from the laser gain section) that does not alter too significantly the ring transmission. We note that this maximum power actually sets the limit to the maximum power that can generate the tunable laser. For this reason the laser in [9] has very limited power from the gain chip and the output power has to be boosted by an additional semiconductor optical amplifier.

Available models of the ring non-linear spectral response in the literature rely on empirical values of carrier lifetimes that are retrieved by fitting experimental measurements [4–6].

The purpose of our study is to present a model which includes, together with non-linearities and self-heating, the formulation of the Shockley-Read-Hall theory for carrier recombination in order to find self-consistently the spectral response of the ring in non-linear regime. Model details are discussed in section 2.

The proposed model is validated in section 3 by comparison with measurements of transmission spectra of two different types of resonators (one micro-ring with small waveguide cross-section and one race-track resonator) realized in separate foundries. The modelling approach is then applied to quantify the maximum power that can enter in the rings of a widely tunable laser similar to the one in [9] whose rings have been designed to guarantee tuning range covering the C-Band, high side-mode suppression ratio (SMSR) and narrow laser linewidth.

2. Model

We consider both a ring and racetrack resonators with schematic structure in Fig. 1; in case of the racetrack configuration L_c is the coupler length and L_d the length of the straight waveguide, r is the curvature radius. For the classic ring configuration we have $L_c = L_d = 0$. The coupler has coupling coefficient κ and transmission coefficient t. The coupling loss in the bus-ring coupling region is indicated with parameter η^2, such that, defining P_{bus} the power entering in the coupler, the power loss per round trip in this region is $\eta^2 \cdot P_{bus}$ [10]. The power conservation in the bus-ring coupling region is therefore $t^2 + \kappa^2(1-\eta^2) + \eta^2 = 1$ from which we get $t^2 = (1-\kappa^2)(1-\eta^2)$.

With this formulation, the power transmission coefficients at the through and drop port are:

$$\begin{aligned} T_{drop} &= \frac{\kappa^4(1-\eta^2)^2 a}{|1 - t^2 a e^{j\theta}|^2} \\ T_{thr} &= t^2 \frac{|1 - (1-\eta^2) a e^{j\theta}|^2}{|1 - t^2 a e^{j\theta}|^2} \end{aligned}, \tag{1}$$

Optics EXPRESS

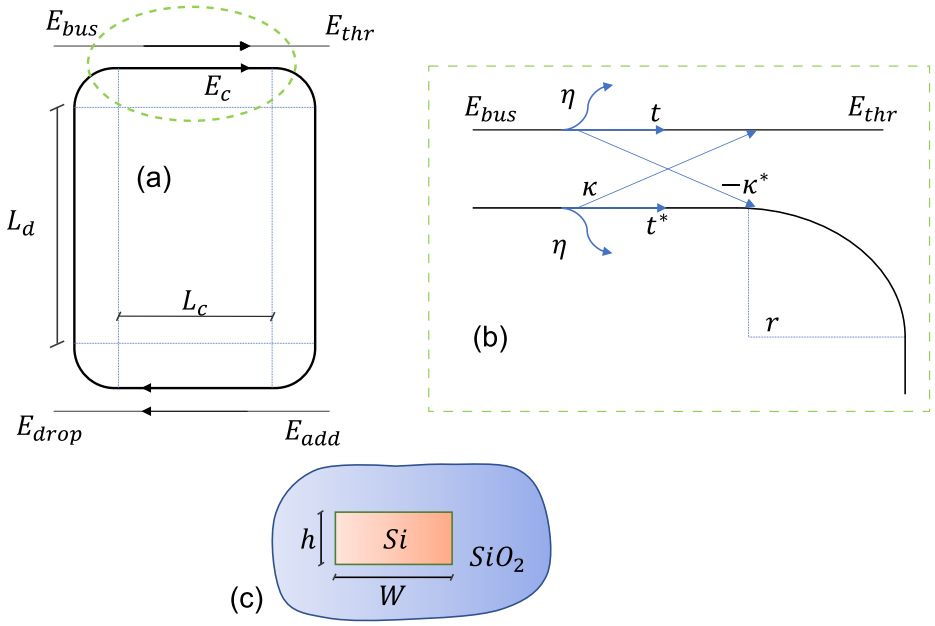

Fig. 1. (a) Schematic of the resonator structure and zoom in the bus-ring coupling region (b). The electric fields at the input bus port (E_{bus}), through port (E_{thr}), add (E_{add}) and drop (E_{drops}) ports are normalized such that $|E|^2$ is a power in Watt. The electric field propagating in the ring waveguide is E_c. The bus and ring waveguide structures and materials are summarised in (c).

whereas the optical power circulating in the ring waveguide can be calculated as:

$$P_c = P_{bus}\frac{\kappa^2(1-\eta^2)}{|1-t^2 a e^{j\theta}|^2}, \tag{2}$$

with P_{bus} the power in the bus waveguide, and θ the total phase variation per round trip:

$$\theta = \theta_0 + \Delta\theta + \frac{n_g}{c}(\omega-\omega_0)L, \tag{3}$$

θ_0 is the phase variation per round trip at the reference angular pulsation ω_0 in linear regime in the waveguide with effective refractive index $n_{eff,0}$ and group refractive index n_g. $\Delta\theta(Pc, \Delta T)$ is the total variation of the phase per round trip due to the non-linear effects and self-heating, which depend on the circulating power and temperature increase as we will discuss in the following.

The modal loss of the optical field per round trip is $a = e^{-\alpha_{eff}L/2}$, here α_{eff} is the loss in the ring waveguide due to linear and non linear effects. Note that the loss at the coupler (i.e. waveguide ring/bus waveguide interface) are accounted with the parameter η^2. We express the effective waveguide loss as: $\alpha_{eff}(P_c) = \alpha_0 + \alpha_{rad} + \Delta\alpha(P_c)$; α_0 is the liner loss term attributed to light scattering, surface state absorption and small residual doping, while α_{rad} is the term accounting for the bend loss and therefore for light radiated in the cladding.

The non-linear part is written as: $\Delta\alpha(P_c) = \alpha_{TPA}(P_c) + \alpha_{FC}(n_e, p_e)$. $\alpha_{TPA}(P_c)$ is the modal loss caused by two-photon absorption, which depends on the power propagating in the ring; α_{FC} is the free-carrier absorption caused by free carrier density (i.e., electron density per unit volume, n_e, in conduction band and hole density per unit volume, p_e, in valence band) generated by TPA [4,11,12]. Similarly $n_{eff}(P_C, \Delta T) = n_{eff,0} + \Delta n_{eff}(P_c, n_e, p_e, \Delta T)$ is the total effective refractive

Optics EXPRESS

index of the silicon core with Δn_{eff} the effective refractive index variation caused by FCD and self-heating.

Two photon absorption is significant in silicon in both C- and O- band [13] and causes accumulation of free carriers. These carriers can then absorb other photons due to free-carrier absorption; as a consequence, they are pushed to higher energies in conduction band or valence band and release heat by relaxing back to their initial state. Eventually free electrons recombine with free holes via Shockley–Read–Hall (SRH) recombination favoured by traps due to defects in the Si bulk material or at the waveguide interface between silica and silicon. Radiative recombination is impossible in silicon, whereas Auger recombination is neglected due to the low density of the generated free carriers [14].

Optical power absorbed by these processes is then dissipated into heat causing a temperature increase ΔT almost confined in the silicon core; hence the silicon refractive index and the waveguide effective refractive index are modified by self-heating [4,5,15].

The aim of this work is the calculation of the ring transmission coefficients for any injected power and wavelength around the cold resonant pulsation ω_0. To solve this non-linear problem, it is convenient to express the resonant denominator as function of the ratio $\frac{P_{bus}}{P_c}$:

$$|1 - t^2 a e^{j\theta}|^2 = \frac{P_{bus}}{P_c}\kappa^2(1-\eta^2) \tag{4}$$

and the transmission coefficients of Eq. (1) as:

$$\begin{aligned} T_{drop} &= \frac{P_c}{P_{bus}}\kappa^2(1-\eta^2)a \\ T_{thr} &= \frac{P_c}{P_{bus}} \cdot \frac{t^2}{k^2} \cdot \frac{|1-(1-\eta^2)ae^{j\theta}|^2 \cdot}{(1-\eta^2)} \end{aligned} \tag{5}$$

We note that the transmission coefficients in Eq. (5) have a non-linear dependence with P_c because of the expressions of a and θ discussed above.

In the rest of this section we will discuss the model of Shockley–Read–Hall (SRH) recombination in order to write a rate-equation for the free carrier density. We will also summarize the model adopted for TPA, FCA and self-heating.

2.1. Model of SRH carrier recombination

The free carrier recombination rate in previous works has always been quantified through a generic recombination term as $\frac{N}{\tau}$, indicating with N the free carrier density and τ a generic lifetime for the recombination process. This simplified recombination model implicitly assumes that electron and hole FC densities are equal (i.e., $n_e = p_e = N$) and the carrier lifetime is a constant value independent on the carrier density and thus on the pumping power.

This very simplifying assumption is not true for the silicon waveguide case; indeed in [16] experimental measurements on Si straight waveguides showed that the FC dynamics is rather non-linear (i.e., very dependent on the optical power in the waveguide). In [16], the authors also demonstrate that the non-linear carrier dynamics can be well explained in the frame of the rigorous SRH recombination theory [17]. The findings in [16] can also justify why in previous works on non-linear ring resonators [4–6] it was necessary to assume an empirical carrier lifetime depending on circulating power to explain measured results.

In this work we couple the non-linear ring model with a rigours model of the SRH recombination where the traps act as recombination/trapping center (trap-assisted recombination) upon the capture/trapping of a hole and an electron. We indicate with N_f the bulk trap density per unit of volume in the silicon waveguide and with E_t the trap energy level inside the energy band gap. The density of surface traps N_s, referred to waveguide side-walls imperfection, can be

Optics EXPRESS

reduced to the equivalent volume density introduced above similarly to what done in [16]; namely, $N_f = N_s \cdot \frac{2(W+h)}{W \cdot h}$ which takes into account that the surface defects are equally distributed over all the contact surface between the silicon core and the SiO_2. The free carrier generation rate per unit volume in the waveguide is $G = \frac{\alpha_{TPA} P_c}{2\hbar\omega A}$, while the rates of variation of excess electron (n_e) and hole (p_e) densities generated by TPA are [17]:

$$\begin{aligned} \frac{\partial n_e}{\partial t} &= G - \frac{1}{\tau_{n0}} \left(\frac{(n_0 + n_1 + n_e)(n_e - p_e)}{N_f} - \frac{n_e n_1}{n_e + n_o} \right) \\ \frac{\partial p_e}{\partial t} &= G - \frac{1}{\tau_{p0}} \left(\frac{(p_0 + p_1 + p_e)(p_e - n_e)}{N_f} - \frac{p_e p_1}{p_e + p_o} \right) \end{aligned}, \tag{6}$$

with $\tau_{n0} = (N_f \sigma_n v_n)^{-1}$, $\tau_{p0} = (N_f \sigma_p v_p)^{-1}$ representing the shortest capture time of carriers in the trap when it is not occupied by electrons and holes. $\sigma_{n,p}$ is the capture cross section, and $v_{n,p}$ the thermal velocity of electrons and holes equal to $2.3 \cdot 10^{15}\, m/s$ and $1.65 \cdot 10^{15}\, m/s$ respectively [18]. We note here that the different capture cross section and thermal velocity of electrons and holes cause a different capture rate in the traps that eventually unbalance electron and hole densities. Thus the simplifying assumption that $n_e = p_e = N$ fails. We also note that in Eq. (6) it is rather difficult to identify a unique carrier lifetime τ; as discussed in the following we can only define equivalent carrier lifetimes once the rate equations in (6) are solved in steady state.

At equilibrium, n_0 and p_0 are electron and hole concentration without considering traps; $n_1 = n_0 e^{(E_t - \psi_f)/k_b T}$ and $p_1 = p_0 e^{(\psi_f - E_t)/k_b T}$ depend on the difference between the Fermi energy level, ψ_f, of the silicon bulk (with a possible residual doping level) and E_t.

In the present study we consider only steady state solutions ($\frac{\partial n_e}{\partial t} = \frac{\partial p_e}{\partial t} = 0$) because, in the experimental results shown in the following section, we report measurements of the ring transmission coefficient varying input wavelength or input power at a rate slower than $1\, ms$ per measurement; in this scenario, any thermal or carrier transient is concluded [16].

In steady state Eq. (6) reduces to two polynomial equations with unknowns n_e and p_e. Through a normalisation with respect to p_0 [17] and defining $y = p_e/p_0$, $x = n_e/p_0$, the equation for holes yields:

$$\begin{aligned} &y^3 + y^2 \left\{ (2 + b + ab) + N_e b/(1 + b) - G_e(1 + \gamma^{-1}) \right\} + \ldots \\ &y \left\{ (1 + b)(1 + ab) + N_e b/(1 + b) - G_e/\gamma(1 + b)(1 + a + 2a/\gamma) - N_e G_e(1 + 2b)/\gamma(1 + b) \right\} - \ldots. \\ &- G_e \left\{ (1 + b)^2(1 + a/\gamma) - N_e(G_e - \gamma)/\gamma^2 \right\} = 0 \end{aligned} \tag{7}$$

Where $a = n_1/p_0$, $b = p_1/p_0$, $G_e = G\frac{\tau_{n0}}{p_0}$, $N_e = N_f/p_0$, $\gamma = \tau_{n0}/\tau_{p0}$, $\tau_{p,n} = p_e, n_e/G$ are all normalised parameters with respect to the hole carrier density at equilibrium.

The previous equation is solved through the search of all trigonometric solutions of a depressed cubic equation with Eq. (7) expressed in the form $a_y y^3 + b_y y^2 + c_y y + d_y = 0$. The solutions y_k with $k = 0, 1, 2$, are then uniquely associated to the excess electron density x_k through the expression:

$$x_k = y_k - \frac{N_e}{\gamma \cdot (y_k + 1 + b)} \left(G_e - \frac{\gamma b y_k}{1 + b} \right), \tag{8}$$

which has been obtained from the hole rate equation in (6). Among the different solutions, only $k = 0$ provides a physically sound solution since it guarantees that the excess electron and hole densities satisfy the condition $0 < (p_{k,e} - n_{k,e})/N_f < 1$ which represents the fraction of occupied traps. For this reason, from now the index k is dropped and it is always equal to 0.

For typical silicon traps, the electron and hole capture times, τ_{n0} and τ_{p0}, are different resulting in an unbalance between electron and hole densities. For any generation rate G_e, we may write an equivalent electron and hole lifetime defined as $\tau_n = n_e/G_e$ and $\tau_p = p_e/G_e$. With this method,

Optics EXPRESS

the hole carrier lifetime can be explicitly written as:

$$\begin{aligned}\tau_p &= \frac{\tau_{n0}}{G_e}\left\{2\sqrt{-\frac{p}{3}}cos\left[\frac{1}{3}\arccos\left(\frac{3q}{2p}\sqrt{-\frac{p}{3}}\right)-2\pi k/3\right]-\frac{b_y}{3a_y}\right\}\\ p &= \frac{3a_yc_y-b_y^2}{3a_y^2}\\ q &= \frac{2b_y^3-9a_yb_yc_y+27a_y^2}{27a_y^3}\end{aligned}, \tag{9}$$

and a similar expression is obtained for electron lifetime.

In the case of very high input power, such that we assume $G_e \to \infty$, we get:

$$\tau_{e,\infty} = \tau_{p,\infty} = \tau_\infty = \tau_{n0}(1+\gamma^{-1}). \tag{10}$$

2.2. Model of non-linear loss and self-heating

Through Eq. (7) and (8) we can calculate the density of free carriers (electrons and holes) generated for a fixed value of circulating power. In this section we provide the expressions for the non-linear modal loss and effective refractive index variation to find self-consistently the circulating power in the ring for a given input wavelength and bus input power. Non-linear loss due to TPA is expressed as [12] :

$$\alpha_{TPA} = \frac{\beta_{TPA}}{A_{eff}}P_c, \tag{11}$$

where $\beta_{TPA} = 0.8\,cm/GW$ is the TPA absorption coefficient in C-band [4,11,13,19]. The effective area A_{eff} is defined accordingly to the model in [12]:

$$A_{eff} = \frac{Z_0^2}{n_{Si}^2}\frac{\left|\int\int_{A_{tot}} \Re e\{E(x,y)\times H(x,y)\}\cdot e_z dxdy\right|^2}{\int\int_A |E(x,y)|^4 dxdy}, \tag{12}$$

where A is the area of the silicon cross section of the waveguide in Fig. 1; A_{tot} is the total area of the simulation domain (including both Si and SiO_2) where the electromagnetic field has been computed. $Z_0 = 377\,\Omega$ is the free-space wave impedance. The optical confinement factor (Γ) in the silicon cross section of the waveguide is [20,21]:

$$\Gamma = \frac{n_{Si}c\epsilon_0\int\int_A |E(x,y)|^2 dxdy}{\int\int_{A_{tot}} \Re e\{E(x,y)\times H(x,y)\}\cdot e_z dxdy}, \tag{13}$$

with e_z the unit vector pointing in the propagation direction z. In eq. (13) and (12), $E(x,y)$ and $H(x,y)$ are the transversal complex electric and magnetic field profiles of the fundamental guided mode; $n_{Si} = 3.48$ is the refractive index of Silicon. These profiles are calculated with an optical mode solver based on the Field-Mode-Matching (FMM) method [22,23], and cross-checked with a Finite-Element-Method solver.

The modal losses due to free-carrier-absorption are expressed as a function of the excess electron and hole densities obtained by the SRH recombination model, through the empirical expressions in [24]:

$$\alpha_{FC} = \Gamma\left(8.88\cdot 10^{-21}n_e^{1.167} + 5.84\cdot 10^{-20}p_e^{1.109}\right). \tag{14}$$

We neglect in our model the variation of silicon refractive index due to TPA because it is negligible compared to the contribution due to FCD and temperature [5]. The effective refractive

Optics EXPRESS

index due to generated free-carriers and temperature is $\Delta n_{eff} = \Delta n_{eff,FCD} + \Delta n_{eff,T}$ with [24]:

$$\Delta n_{eff,FCD} = -\Gamma(5.4 \cdot 10^{-22} n_e^{1.011} + 1.53 \cdot 10^{-18} p_e^{0.838}). \tag{15}$$

The coefficients reported in Eq. (14) and Eq. (15) are for C-band, while n_e and p_e are expressed in $[cm^{-3}]$. For what regards the thermal effect, its derivation is similar to [4,5,15]. The power dissipated by the ring, P_d, is expressed as $P_d = P_{rad} + P_{abs}$, where P_{rad} represents the light lost radiated in the cladding and P_{abs} is the absorption contribution which is associated to the conversion into heat. The radiated power can be written as:

$$P_{rad} = \eta^2 \cdot (P_{in} + P_c \cdot (a + a^2 \cdot t)) + P_c(1 - a_{rad})(1 + t^2 \cdot a). \tag{16}$$

The first term at the RHS is associated to the power lost at the coupler whereas the second term is power lost due to ring bend and therefore radiated in the cladding with $a_{rad} = e^{-\alpha_{rad} \cdot L/2}$. The power absorbed in the core is due to TPA, FCA and also waveguide loss α_0 [4,5,15,25]. As we will show in the comparison of the model results with the experimental measurements, the inclusion of the linear loss term α_0 in the power absorbed is essential to fit the experiments at low input power; this means that photon absorption in the core, mainly due to surface state absorption [8], is the most dominant contribution to the waveguide loss α_0. The absorbed power can be written as:

$$P_{abs} = P_c(1 - a_{abs})(1 + t^2 \cdot a), \tag{17}$$

with $a_{abs} = e^{-(\alpha_0 + \Delta\alpha(P_c)) \cdot L/2}$. Finally the absorbed power is converted into heat changing the effective refractive index of silicon through the relation:

$$\Delta n_{eff,T} = \Gamma \frac{dn_{Si}}{dT} Z_T P_{abs}. \tag{18}$$

Here $\frac{dn_{Si}}{dT} = 1.86 \cdot 10^{-4}\, K^{-1}$ is the silicon thermo-optic coefficient [4] and Z_T the thermal impedance of the ring.

2.3. Numerical solution

By inserting in Eq. (2) all the expressions derived above for the effective loss α_{eff} and phase variation $\Delta\theta$ as function of P_{bus} and P_c, we note that Eq. (2) is a complex non-linear equation with unknown P_c. We have solved this equation numerically to get the circulating power for a fixed bus power at any input wavelength λ. From the circulating power, we then get the effective loss and the transmission coefficient. When bi-stability occurs, the non-linear equation can have up to three distinct possible solutions [15]. Experimentally only two cases are observable: one that corresponds to the stable state obtained by increasing the injected wavelength with respect to a previous stable state (i.e., wavelength sweep from blue to red), whereas the other solution is found with the opposite wavelength sweep (i.e., from red to blue) [5,12,15]. The calculated solutions representing a forward wavelength sweep (i.e., from blue to red wavelength) for different bus power are used in the next section to compare our model with measured transmission coefficients at different input wavelengths and bus powers.

3. Results

To validate our model, in this section we compare the measured transmission spectra of two resonator structures (ring A and racetrack B) that differ for waveguide cross section, length, coupling coefficients κ^2 and foundry for the fabrication as summarized in Table 1.

For Ring A we have measured transmission coefficients at ring through port around the resonance wavelength $\lambda_0 = 1554\,nm$, whereas in the case of Racetrack B we have selected the resonance at $\lambda_0 = 1540\,nm$.

Optics EXPRESS

Table 1. Parameters used in the model retrieved from the fitting of the rings transmission spectra at low input power and from electromagnetic mode solver.

Parameter	Ring A ($\lambda_0 = 1554\,nm$)	Racetrack B ($\lambda_0 = 1540\,nm$)	Unit	Source
L	31	80	μm	-
W	580	450	nm	-
h	107	215	nm	-
Γ	0.679	1	-	Electromagnetic mode solver
A_{eff}	0.1089	0.075	μm^2	Eq. (12)
$n_{eff,0}$	1.911	2.33	-	Electromagnetic mode solver
n_g	3.38	4.26	-	Electromagnetic mode solver
κ^2	0.037	0.065	-	Fitting of $T_{thr}(\lambda)$ in linear regime
α_0	1.09	2	dB/cm	Fitting of $T_{thr}(\lambda)$ in linear regime
α_{rad}	3.57	<0.01	dB/cm	Electromagnetic mode solver
η^2	0.002	0.004	-	Fitting of $T_{thr}(\lambda)$ in linear regime
Q	5672	9421	-	Fitting of $T_{thr}(\lambda)$ in linear regime

To measure the ring transmission coefficients in the non-linear regime, the power from a tunable laser is injected in the bus waveguide; the transmission coefficient at the through port is measured as the ratio between the power in the bus waveguide and the power measured at the through port of the ring. Such spectrum is measured by sweeping the tunable laser wavelength from blue to red wavelengths around one selected resonant wavelength of the ring λ_0. An Agilent 81980A was used to characterise ring A with a sweeping rate of $5nm/s$. In the case of racetrack B, an Agilent 8168A tunable laser has been used for low power characterisation with a sweeping rate of $3pm/s$. A relatively low sweeping rate was adopted in order to ensure that any thermal transient is concluded. Due to the limited output power of the Agilent 8168A tunable laser, a second tunable laser (four port tunable laser N7714A) was employed for the characterisation of racetrack B at high input powers.

3.1. Fitting of measured transmission coefficients

To reproduce the measured transmission coefficients, we must select in our model some fitting parameters; these are the density of traps N_f, their energy level E_t and the thermal impedance Z_T. We fix the thermal impedance close to values obtained from thermal simulation of both resonators. For what concerns the SRH model and parameters quantifying the capture dynamics of carriers in the traps, we consider donor type traps with non degenerate energy level [16] which are usually assumed to be close to the middle of the band gap [15–17,25]; as a result we vary E_t from $0.6eV$ to $0.7eV$. The electron capture cross section for donor type trap is a function of the energy of the traps (i.e., $\sigma_n(E_t)$), we extrapolate this function for energies above the mid-gap from measurements reported in [6]. Lastly, we fix the residual doping of silicon to $N_a = 10^{15}\,cm^{-3}$ following the technology guidelines by the foundry and corresponding to $\psi_f \approx 0.23\,eV$.

As reported in the literature [6,16], it is not possible to measure both the electron and hole capture cross sections when the trap energy level is far from the mid-gap; as a consequence, we suppose $\gamma = 0.05$ which was estimated from the ratio of measured cross-sections when E_t is at mid-gap [6]. Therefore even in the case of mid-gap traps the assumption of equal electron and hole capture cross-section is generally incorrect. For what concerns the trap densities, they have been varied so that the calculated surface trap densities correspond to values in the range $10^{10} - 10^{12} cm^{-2}$ [16].

The measured variation, with increasing P_{bus}, of the ring resonant wavelength and transmission coefficient at resonance were chosen as target values for the fitting procedure that finds N_f and E_t

Optics EXPRESS

by minimizing the relative error defined as the difference between the measured and simulated variation of resonant wavelength and transmission coefficient.

For the case of ring A, we set the thermal impedance to $Z_T = 18900\,K/W$ that has been obtained by thermal simulations of the entire ring structure including the SiO_2 buried oxide and the silicon substrate. Figure 2(a) and 2(b) report with symbols the shift of the resonant wavelength $\Delta\lambda = \lambda_{res} - \lambda_0$ (with λ_{res} being the resonant wavelength modified by NL effects and self-heating) and the transmission coefficient at resonance extracted from the measured transmissions, versus the input bus power. These measured data form the target curves we have considered in the fitting procedure. The continuous line is the simulation result obtained with $N_f = 4 \cdot 10^{16}\,cm^{-3}$, $E_t = 0.63\,eV$, The calculated surface trap density is $N_s = 1.81 \cdot 10^{11}\,cm^{-2}$ that is in agreement with experimental measurements on Si/SiO_2 interfaces [6,26].

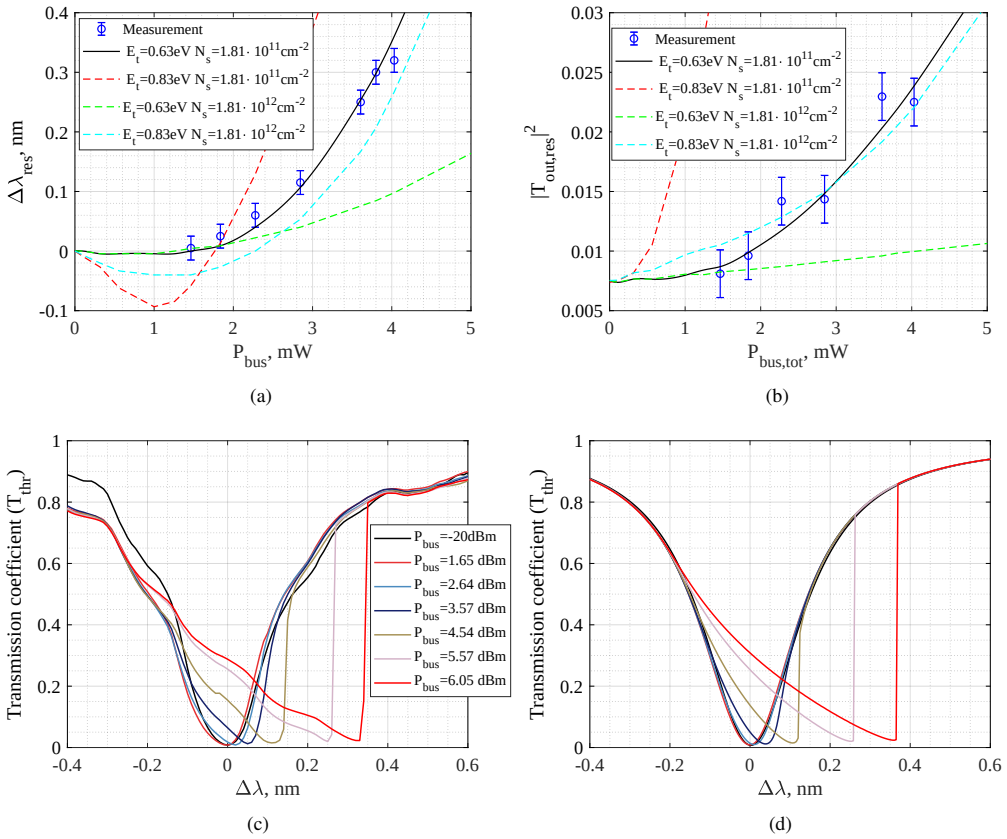

Fig. 2. Resonant wavelength shift $\Delta\lambda$ (a) and variation of the transmission coefficient at resonance (b) as a function of the input bus power. Simulation results obtained with our SRH model are in solid line, whereas dashed lines are calculated assuming different combination of energy trap level E_t and surface trap densities N_s. Transmission coefficients at different input bus power measured (c) and simulated (d) by sweeping the input wavelength from the blue to red side of the resonant wavelength. The simulated spectrum was obtained with $E_t = 0.63eV$ and $N_s = 1.81 \cdot 10^{11}cm^{-2}$. The color legend in (d) is the same of (c).

The measured and simulated transmission spectra are shown in Fig. 2(c) and 2(d) for different bus input powers. Here, the black curve corresponds to a low input power which results in a linear response of the ring. For increasing P_{bus}, the circulating power increases leading to higher propagation loss and variation of silicon refractive index. These cause first a slight blue shift

Optics EXPRESS

of the resonant wavelength due to FC effect being dominant over the temperature rise, then a significant red shift caused by self-heating. The figure shows that the model can reproduce well measured results through an accurate definition of the fitting parameters.

In Fig. 2(a) and Fig. 2(b) the results of the model for different combinations of trap energy level and trap density are also displayed with dashed lines. We clearly see that these two parameters play an important role in defining the carriers dynamics that determines the density of free carriers and therefore the shift of the resonant wavelength and the degradation of the transmission coefficient. For example with mid-gap traps ($Et = 0.63eV$) the increase of trap density leads to a reduction of the non-linear absorption and self-heating because the FC can recombine faster and less FC are available for free-carrier absorption. On the contrary, at low trap density ($N_s = 1.81 \cdot 10^{11} cm^{-2}$) the FC absorption and dispersion are effective even at low power because the holes generated by TPA can hardly recombine with the electrons that are captured in the trap states.

To understand better this concept, it is useful to plot the equivalent electron and holes lifetimes as defined in Eq. (9) as function of the circulating power in the ring. These are reported in Fig. 3(a) and (b). The trend in the figure shows that the unbalance of electron and hole capture rates in the trap state, and the consequent unbalance of electron and hole free carrier densities, leads to carrier lifetimes that are power dependent (i.e., non-linear carrier lifetime); which is in agreement with [4–6] where a dependence of carrier lifetime on illumination power was assumed to explain experimental results. Figure 3(a) and (b) clearly show that the rate of electron and hole lifetimes variation with P_c significantly depends on the energy trap level and on the surface trap density.

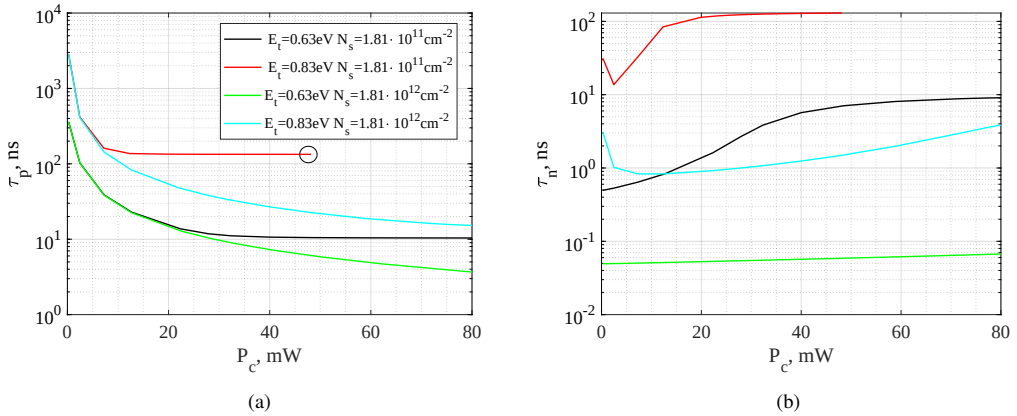

Fig. 3. Free-carrier lifetime of holes (a) and electrons (b) versus circulating power at the resonant wavelength for different values of surface trap density and trap energy level. The circled pint in (a) represents the circulating power obtained for a bus power equal to $6dBm$ in the specific case of $E_t = 0.83eV, N_s = 1.81 \cdot 10^{11} cm^{-2}$. Such power corresponds to $P_c = 80mW$ in the remaining three cases. The color legend in (b) is the same of (a).

Here the lifetimes of holes and electrons are displayed for different trap energy levels and densities, these curves are associated to the fitting displayed in Fig. 2(a) and (b). When we have $E_t = 0.83eV, N_s = 1.81 \cdot 10^{11} cm^{-2}$ the equivalent electron and holes lifetimes are very large, i.e., $\tau_{p,n}$>$100ns$; as a result the propagating field inside the cavity suffers important loss due to FCA. This is also enlightened by the fact that for a bus power of $6dBm$, the calculated P_c is around $42mW$ which is almost half the circulating power we would obtain for the same P_{bus} in all other cases shown in the figure, i.e., $P_c = 80mW$. We also note that $\tau_{n,p}$ reaches a constant and equal value when P_c is high enough, reflecting the saturation of filled traps, where the number

Optics EXPRESS

of generated free-carriers exceeds the total quantity of traps. This also happens when P_c is about $40\,mW$ in the case of $E_t = 0.6\,eV$ and $N_s = 1.81 \cdot 10^{11} cm^{-2}$ that resulted in being the best fitting parameters to reproduce the experimental measurements of Ring A. For the latter, using Eq. (10) we get that $\tau_\infty \approx 10ns$ from which we understand that in ring A the approximation of a constant and equal lifetime for both electrons and holes for power in the bus larger than $2mW$, (i.e. $P_c \approx 40mW$) is possible and is as a direct consequence of the saturation of available traps at Si/SiO_2 interfaces.

In this particular case we verified that the experimental data could be satisfactorily fit also with a unipolar model for free carriers (i.e,: $n_e = p_e = N$) with a constant carrier lifetime $\tau = 10ns$. However this cannot be considered a general conclusion: if the trap density was higher, the hypothesis that electron and hole lifetimes are equal and constant with circulating power would have been no longer valid (see for example the green lines in Fig. 3).

Figure 4(a) and (b) give further insight into the impact of the trap energy levels on the values of carrier lifetimes and how they depend on the circulating power. More precisely, Fig. 4(a) shows how the carrier lifetimes for $N_s = 1.81 \cdot 10^{11} cm^{-2}$ change with trap energy level approaching the conduction band. The electrons capture cross section are $\sigma_n = 2.18 \cdot 10^{-15} cm^2$ for $E_t = 0.63\,eV$, $\sigma_n = 1.69 \cdot 10^{-16} cm^2$ for $E_t = 0.83\,eV$, and $\sigma_n = 3.79 \cdot 10^{-18} cm^2$ for $E_t = 1\,eV$ as extracted from the measurements displayed in the inset of Fig. 4(a). We note how the capture cross section of electrons (and of holes consequently) decreases with increasing E_t; as a result, even if the traps are closer to the conduction band, the very small capture cross section results in a lower probability for a trap to capture an electron and make it recombining with the hole. The number of generated free carriers in the ring resonator will be higher than in the case with smaller E_t leading to important loss and decrease in circulating power as explained before. For this reason at $E_t = 1\,eV$ the carrier lifetimes are high and become constant at rather small values of P_c.

The same result is obtained when reducing the surface trap density (Fig. 4(b)) for E_t fixed at $0.63eV$. In this case it is clear that the lower is the surface trap density, the faster the traps will be all filled by carriers making the lifetimes reach a constant value at smaller circulating power.

To complete the description, Fig. 4(c) summarises the contributions of free-carriers and temperature to the overall refractive index shift in the silicon waveguide for the parameters $E_t = 0.63eV$ and $N_s = 1.81 \cdot 10^{11} cm^{-2}$ that fit the experimental measurements of ring A. The FC contribution is plotted with reverse sign in order to compare it with the temperature contribution. For low circulating power, i.e. P_c<$40\,mW$, the heating due to linear absorption and non-linear losses gives a contribution comparable with the FC generation. For this reason we do not observe a significant increase in the $\Delta\lambda$ up to a bus power of about $2\,mW$ in Fig. 2(a) . We denote that the reported values of the variation of refractive index due to temperature and FCD are close to those reported in [5] for similar cavity power, i.e. circulating power in the ring resonator.

To further validate our approach, we consider racetrack B, having a quality factor higher than ring A, and we apply the model to reproduce its measured spectral response.

The measurements and simulation results of the resonant wavelength shift and variation of transmission coefficient with bus power are reported in Fig. 5(a) and 5(b) respectively, while the measured and calculated transmission spectra are in (c) and (d). Fitting parameters for resonator B are $Z_T = 4600\,K/W$, $N_s = 7.4 \cdot 10^{10}\,cm^{-2}$ and trap energy level around $0.69\,eV$. The thermal impedance for fitting is only 10% different from the one simulated with the thermal simulations that was $Z_T = 5044K/W$. The residual p-doping is the same we assumed for Ring A.

The error bars in Fig. 5(a) and 5(b) up to $2\,mW$ are found by collecting the variance over a series of transmission coefficient measurements repeated on the same device. The larger error bars for P_{bus}>$2.1mW$ are related to the reduced wavelength accuracy ($\approx \pm 22pm$ against $5pm$) and instability of the second high power tunable laser we had to employ for the high power measurements of racetrack B. Nonetheless also in the case of racetrack B we get a good agreement of the model with the experiments as also confirmed by the comparison of measured

Optics EXPRESS

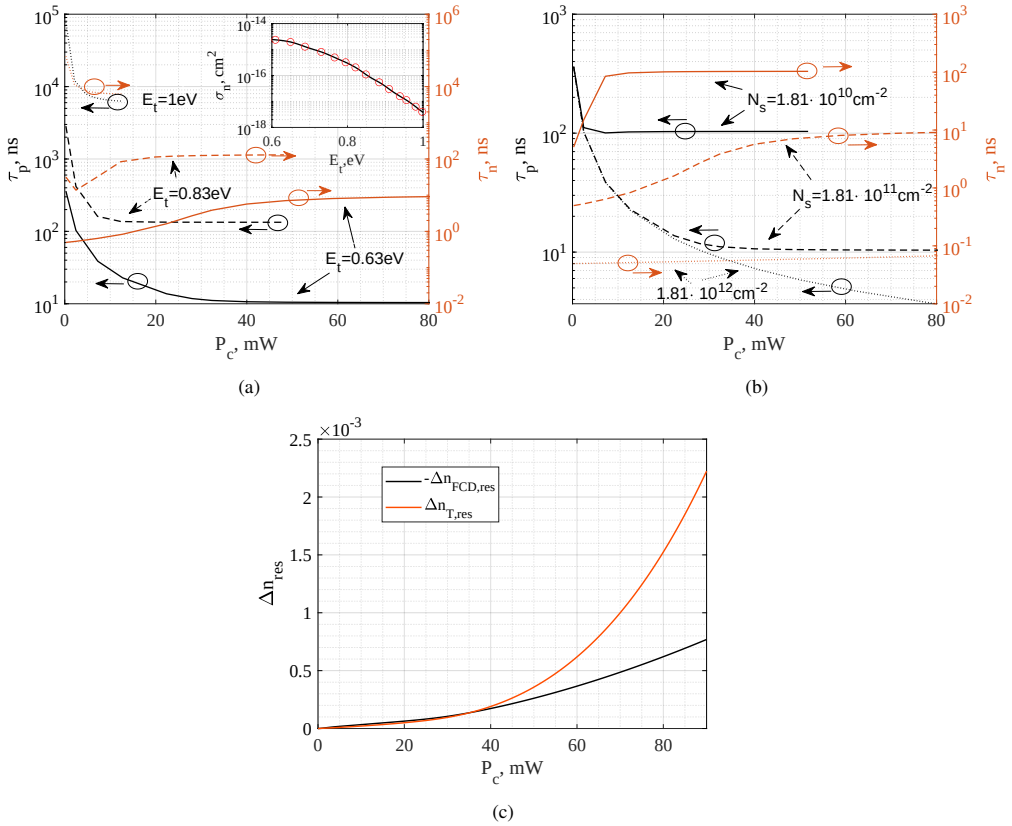

Fig. 4. (a) Free-carrier lifetime of holes and electrons versus circulating power at resonant wavelength for different trap energy level in the case of $N_s = 1.81 \cdot 10^{11} cm^{-2}$. In the inset of (a), the electron capture cross section versus E_t from [6] is displayed. (b) Free-carrier lifetime of holes and electrons for different surface trap densities when $E_t = 0.63eV$. (c) Contributions to the effective refractive index change of free-carriers and temperature when $E_t = 0.63eV$ and $N_s = 1.81 \cdot 10^{11} cm^{-2}$. The FC contribution is displayed with reverse sign to better compare the magnitude of the two effects

and simulated transmission spectra in Fig. 5(a) and (b). The red bars in Fig. 5(c) refers to instability in the output transmission due to periodic oscillation of the output power at through port that are observed when bus power is high enough. This oscillating response of the ring is caused by periodic oscillations of the ring resonant wavelength caused by the interplay of generated free carriers and self-heating [5,25]; the strength and periodicity of the oscillations depend on the detuning between the input wavalength and cold resonant wavelength (i.e., $\lambda_{in} - \lambda_0$) and on the bus power.

For this structure the saturated equivalent carrier lifetime is equal to $\tau_\infty = 71\,ns$ which is very close to values obtained from fitting of dynamic measurements for a similar ring resonator structure [25]; in our case the free carrier density at $P_{bus} = 6.4dBm$ is similar for both electrons and holes and equal to $3 \cdot 10^{17} cm^{-3}$. It is interesting to observe how the model reproduces well the positive wavelength shift measured at low input power less than $1\,mW$: this shift is caused by the linear absorption (due to contribution of α_0) that turns in a small self-heating. If the linear loss term α_0 was excluded as contribution to the absorbed power, it would have been impossible to reproduce this initial red shift. By increasing input power the wavelength shift reduces again

Optics EXPRESS

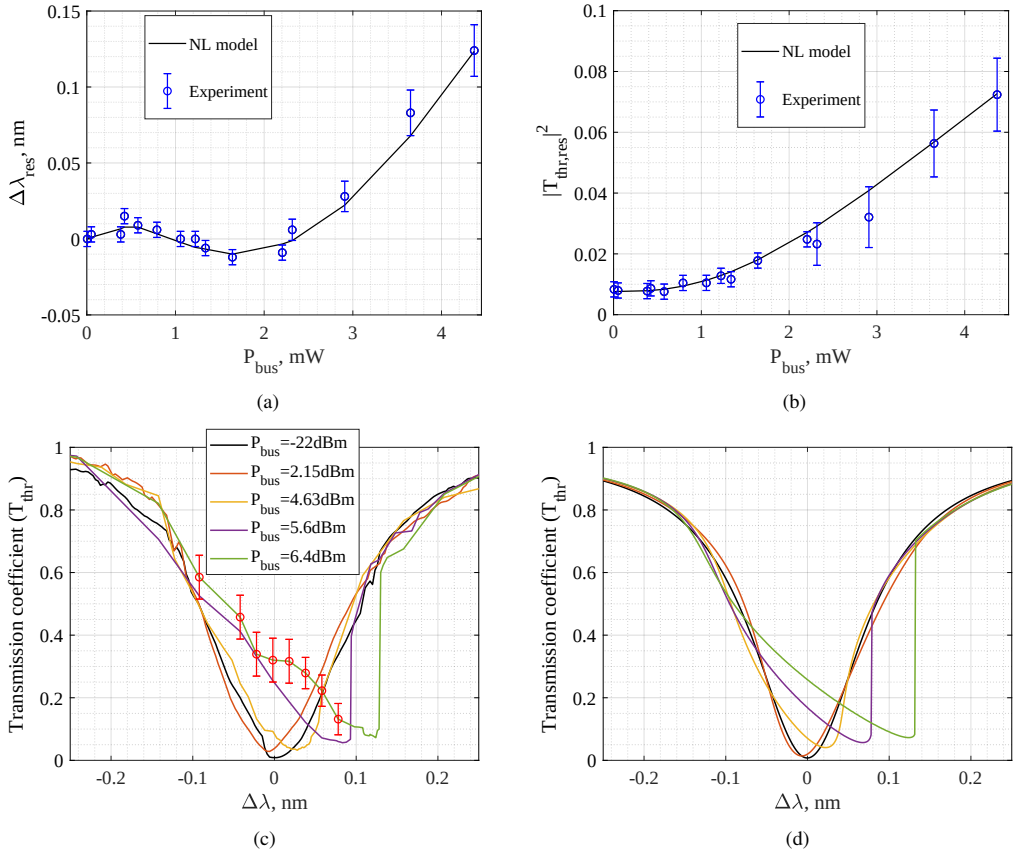

Fig. 5. Resonant wavelength shift $\Delta\lambda$ and variation of the transmission coefficient at resonance (b) in the case of a racetrack ring resonator. Simulation results obtained with our SRH model are in solid line. Transmission coefficients at different input bus power: measured (c) and simulated (d) with a forward wavelength sweep. In Fig. (c) the red bars indicate uncertainty in the measured transmission coefficient due to oscillations of the output power caused by instability of the ring resonance wavelength. The color legend in (d) is the same of (c).

Optics EXPRESS

because the FC dispersion counteracts the self-heating. Only for a further increase of input power we then observe an important contribution of self-heating now dominated by TPA and FCA.

3.2. Ring design

Ring resonators find applications in the realization of widely tunable and narrow linewidth lasers, but due to silicon TPA and FCA, silicon nitride rings are employed instead (for example [27]). Those designs relying on silicon rings provide limited output power that has to be boosted by an additional semiconductor optical amplifier ([9]). The question is therefore what is the maximum input bus power (which is generated by the gain chip) that Si micro-rings can handle without a significant degradation of the ring transmission.

In this section we present a design of silicon micro-rings that can be employed as filters in a widely tunable laser similar to the one in [9]. Based on the model we presented in [28] we report in Fig. 6 the calculated tuning range (Fig. 6(a)), the SMSR (Fig. 6(b)) and the laser linewidth at 4.7 times the threshold current (Fig. 6(c)) as function of the ring coupling coefficient in the case the design employs silicon rings similar to ring resonator A of Table 1. The radius of the two rings ($R1$ and $R2$) providing wide tunability based on the Vernier principle are selected equal to $R1 = 20\mu m$ and $R2$ as reported in Fig. 6(a) to guarantee a ring free spectral range (FSR) such that the tuning range is sufficient to cover the C-band and that the maximum ring heating, which is required to tune thermally the resonant wavelength over the FSR, is about $45°C$. To design the ring coupling coefficients we calculate the laser SMSR, defined as the ratio between the lasing mode power and the power of the other longitudinal mode that lay at the wavelength of the partial overlap of the other two nearest resonances. The value of $R_1 = 20\,\mu m$ is chosen as the best trade-off between the ring FSR (and hence tuning range), maximum temperature increase to cover the FSR and laser SMSR. Detailed expressions for this design are summarized in Supplement 1. We focus our analysis on the ring with radius $R1$ since, being smaller than the second ring, it has a slightly higher P_c for the same P_{bus}.

For the radius $R1$ and coupling coefficients of Fig. 6, we calculate in Fig. 7(a) the maximum power incident in the ring, $P_{bus,max}$, such that the degradation of the ring quality factor (shown for example for $\kappa^2 = 0.2$ in Fig. 7(b)) does not exceed 10%. It is important to remind that $P_{bus,max}$ determines the maximum power we can extract from the tunable laser in the configuration reported in [28].

Figure 7(b) shows how the quality factor degrades with increasing power in the bus in the case $\kappa^2 = 0.2$: with increasing surface trap density the carriers are more easily trapped resulting in a lower total free carrier density. As a result FCA, FCD and self-heating caused by FCA are reduced.

Thanks to our model we can quantitatively predict how this maximum depends on the trap density for a fixed trap energy around the midgap and we evidence how the designs with high SMSR and narrow linewidth necessarily imply a limited P_{bus} that can be quantified with our approach. We stress here that this calculation is impossible in absence of a detailed SRH model that correctly quantifies the carrier lifetimes.

Optics EXPRESS

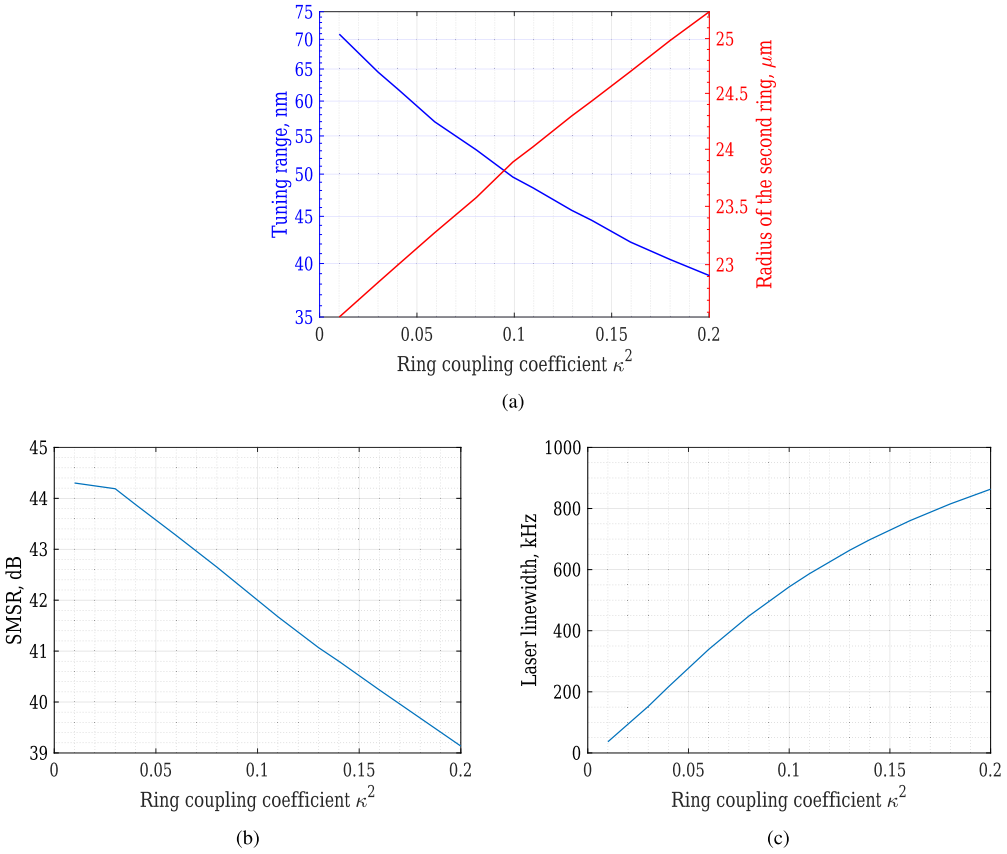

Fig. 6. (a) Calculated tuning range and radius of the second ring as a function of the ring coupling coefficient; (b) SMSR and laser linewidth (c) at about 4.7 time the threshold current versus the ring coupling coefficient.

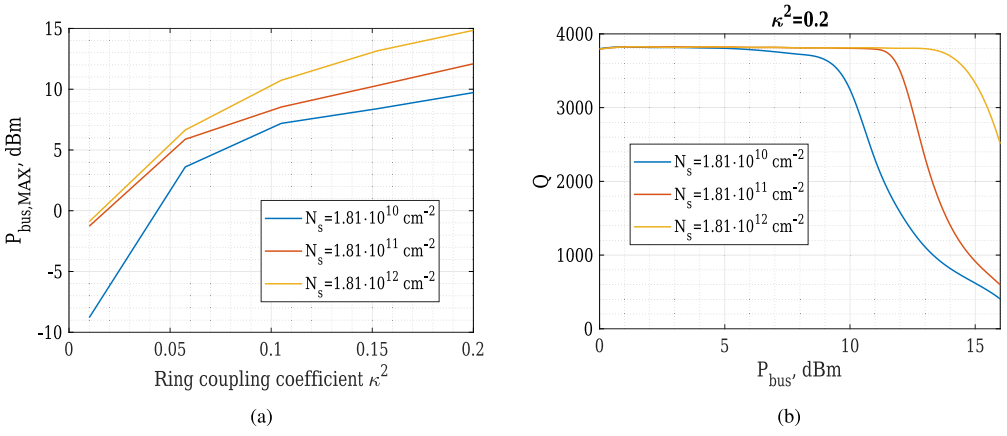

Fig. 7. (a) Maximum allowed bus power, as a function of the coupling coefficient and for different surface trap densities, to limit the reduction of the ring Q-factor to 10% . (b) Example of the quality factor degradation versus P_{bus} in the case $\kappa^2 = 0.2$.

Optics EXPRESS

4. Conclusion

We have presented a new model accounting for non-linear effects in silicon ring resonators with the inclusion of the Shockley–Read–Hall theory. Through trap-assisted recombination, we demonstrate that free carrier lifetimes are strongly dependent on the power circulating in the ring and the way the electron and hole lifetimes depend on power is determined by the trap density and energy level.

This model is essential to have a good fitting of the distortion of the ring transmission spectra with increasing power. Such result is in accord with previous published papers, but in this work it has been obtained without any empirical expressions for the carrier lifetimes.

For the resonators analyzed here and the considered input powers, hole and electron carrier lifetimes result in the range $10 - 100\,ns$. The overall results highlight that surface trap densities around $10^{10} - 10^{11}\ cm^{-2}$ play a crucial role in defining the carrier lifetime in these sub-micron waveguides, and show that the surface trap density and energy level of traps have a non-negligible impact on the ring resonator performances and behaviour. We have also proved the potential of the model in quantifying the maximum power that the silicon rings can handle when they are employed as filters and mirrors in widely tunable and narrow linewidth lasers. The present approach is a first step toward the development of a tool for the design of waveguide cross sections and rings optimized for minimizing the impact of non-linear effects in silicon. For example our results suggest that by an ad-hoc increase of the trap density via implantation of defects [14] we could reduce the impact of the non-linear effects and increase the power that the ring can handle. We also expect that our approach could be useful in the design of rings with waveguide cross sections different from the rib waveguide by employing for example ridge and/or p-i-n waveguides with voltage bias to remove the generated free carries. In this case the SRH model should be coupled with bipolar drift-diffusion continuity equations in order to accurately predict the effective value of the carrier lifetime in these other waveguide structures.

Funding. This work has been supported by a Cisco Sponsored Research Agreement.

Acknowledgements. M. Gioannini and M. Novarese thank Prof. Paolo Bardella (Politecnico di Torino) for sharing the racetrack resonator chip and Dr. Giuseppe Giannuzzi (Politecnico di Bari) for technical help in the experimental part.

Disclosures. The authors declare no conflicts of interest.

Data availability. Data underlying the results presented in this paper are not publicly available at this time but may be obtained from the authors upon reasonable request.

Supplemental document. See Supplement 1 for supporting content.

References

1. W. Bogaerts, P. De Heyn, T. Van Vaerenbergh, K. De Vos, S. Kumar Selvaraja, T. Claes, P. Dumon, P. Bienstman, D. Van Thourhout, and R. Baets, "Silicon microring resonators," Laser Photonics Rev. **6**(1), 47–73 (2012).
2. B. J. Frey, D. B. Leviton, and T. J. Madison, "Temperature-dependent refractive index of silicon and germanium," in *Optomechanical Technologies for Astronomy*, vol. 6273 E. Atad-Ettedgui, J. Antebi, and D. Lemke, eds., International Society for Optics and Photonics (SPIE, 2006), pp. 790–799.
3. H. Nejadriahi, A. Friedman, R. Sharma, S. Pappert, Y. Fainman, and P. Yu, "Thermo-optic properties of silicon-rich silicon nitride for on-chip applications," Opt. Express **28**(17), 24951–24960 (2020).
4. P. E. Barclay, K. Srinivasan, and O. Painter, "Nonlinear response of silicon photonic crystal microresonators excited via an integrated waveguide and fiber taper," Opt. Express **13**(3), 801–820 (2005).
5. G. Priem, P. Dumon, W. Bogaerts, D. V. Thourhout, G. Morthier, and R. Baets, "Optical bistability and pulsating behaviour in silicon-on-insulator ring resonator structures," Opt. Express **13**(23), 9623–9628 (2005).
6. A. G. Aberle, S. Glunz, and W. Warta, "Impact of illumination level and oxide parameters on shockley–read–hall recombination at the si-sio2 interface," J. Appl. Phys. **71**(9), 4422–4431 (1992).
7. Q. Xu and M. Lipson, "Carrier-induced optical bistability in silicon ring resonators," Opt. Lett. **31**(3), 341–343 (2006).
8. Y. Li and A. W. Poon, "Characterization of surface-state absorption in foundry-fabricated silicon ridge waveguides at 1550 nm using photocurrents," in *2016 Conference on Lasers and Electro-Optics (CLEO)*, (2016), pp. 1–2.
9. Y. Gao, J.-C. Lo, S. Lee, R. Patel, L. Zhu, J. Nee, D. Tsou, R. Carney, and J. Sun, "High-power, narrow-linewidth, miniaturized silicon photonic tunable laser with accurate frequency control," J. Lightwave Technol. **38**(2), 265–271 (2020).

Optics EXPRESS

10. C.-W. Tseng, C.-W. Tsai, K.-C. Lin, M.-C. Lee, and Y.-J. Chen, "Study of coupling loss on strongly-coupled, ultra compact microring resonators," Opt. Express **21**(6), 7250–7257 (2013).
11. T. K. Liang and H. K. Tsang, "Role of free carriers from two-photon absorption in raman amplification in silicon-on-insulator waveguides," Appl. Phys. Lett. **84**(15), 2745–2747 (2004).
12. C. Koos, L. Jacome, C. Poulton, J. Leuthold, and W. Freude, "Nonlinear silicon-on-insulator waveguides for all-optical signal processing," Opt. Express **15**(10), 5976–5990 (2007).
13. M. Dinu, F. Quochi, and H. Garcia, "Third-order nonlinearities in silicon at telecom wavelengths," Appl. Phys. Lett. **82**(18), 2954–2956 (2003).
14. S. Park, K. Yamada, T. Tsuchizawa, T. Watanabe, H. Shinojima, H. Nishi, R. Kou, and S. ichi Itabashi, "Influence of carrier lifetime on performance of silicon p-i-n variable optical attenuators fabricated on submicrometer rib waveguides," Opt. Express **18**(11), 11282–11291 (2010).
15. M. Soltani, Q. Li, S. Yegnanarayanan, and A. Adibi, "Improvement of thermal properties of ultra-high q silicon microdisk resonators," Opt. Express **15**(25), 17305–17312 (2007).
16. I. Aldaya, A. Gil-Molina, J. L. Pita, L. H. Gabrielli, H. L. Fragnito, and P. Dainese, "Nonlinear carrier dynamics in silicon nano-waveguides," Optica **4**(10), 1219–1227 (2017).
17. J. Blakemore, *Semiconductor Statistics*, Dover Books on Physics Series (Dover, 2002).
18. "Electrical properties of silicon(si)," http://www.ioffe.ru/SVA/NSM/Semicond/Si/.
19. A. D. Bristow, N. Rotenberg, and H. M. van Driel, "Two-photon absorption and kerr coefficients of silicon for 850–2200nm," Appl. Phys. Lett. **90**(19), 191104 (2007).
20. J. T. Robinson, K. Preston, O. Painter, and M. Lipson, "First-principle derivation of gain in high-index-contrast waveguides," Opt. Express **16**(21), 16659–16669 (2008).
21. T. Visser, H. Blok, B. Demeulenaere, and D. Lenstra, "Confinement factors and gain in optical amplifiers," IEEE J. Quantum Electron. **33**(10), 1763–1766 (1997).
22. A. S. Sudbo, "Film mode matching: a versatile numerical method for vector mode field calculations in dielectric waveguides," Pure Appl. Opt. **2**(3), 211–233 (1993).
23. D. de zutter, P. Lagasse, J. Buus, T. Young, and B. Dillon, "Comparison of different modelling techniques for longitudinally invariant integrated optical waveguides," IEE Proc.-D: Control Theory Appl. **136**(6), 273–280 (1989).
24. M. Nedeljkovic, R. Soref, and G. Z. Mashanovich, "Free-carrier electrorefraction and electroabsorption modulation predictions for silicon over the 1–14-μm infrared wavelength range," IEEE Photonics J. **3**(6), 1171–1180 (2011).
25. M. Borghi, D. Bazzanella, M. Mancinelli, and L. Pavesi, "On the modeling of thermal and free carrier nonlinearities in silicon-on-insulator microring resonators," Opt. Express **29**(3), 4363–4377 (2021).
26. P. J. Caplan, E. H. Poindexter, B. E. Deal, and R. R. Razouk, "Esr centers, interface states, and oxide fixed charge in thermally oxidized silicon wafers," J. Appl. Phys. **50**(9), 5847–5854 (1979).
27. Y. Fan, A. van Rees, P. J. M. van der Slot, J. Mak, R. M. Oldenbeuving, M. Hoekman, D. Geskus, C. G. H. Roeloffzen, and K.-J. Boller, "Hybrid integrated inp-si3n4 diode laser with a 40-hz intrinsic linewidth," Opt. Express **28**(15), 21713–21728 (2020).
28. L. Columbo, J. Bovington, S. Romero-Garcia, D. F. Siriani, and M. Gioannini, "Efficient and optical feedback tolerant hybrid laser design for silicon photonics applications," IEEE J. Sel. Top. Quantum Electron. **26**(2), 1–10 (2020).